AGU PUBLICATIONS

JGR

Journal of Geophysical Research: Atmospheres

RESEARCH ARTICLE
10.1002/2015JD024478

Key Points:
- Flash flood storms are a mixture of intense-convection events and low-echo-centroid events
- Collapse of storm cells is the common feature for flash flood storms
- Extreme rainfall rates are produced by convective systems with wide convective intensity spectrum

Correspondence to:
L. Yang,
longyang@princeton.edu

Citation:
Yang, L., J. Smith, M. L. Baeck, B. Smith, F. Tian, and D. Niyogi (2016), Structure and evolution of flash flood producing storms in a small urban watershed, *J. Geophys. Res. Atmos.*, *121*, 3139–3152, doi:10.1002/2015JD024478.

Received 10 NOV 2015
Accepted 11 MAR 2016
Accepted article online 22 MAR 2016
Published online 6 APR 2016

Structure and evolution of flash flood producing storms in a small urban watershed

Long Yang[1,2], James Smith[1], Mary Lynn Baeck[1], Brianne Smith[3], Fuqiang Tian[2], and Dev Niyogi[4]

[1]Department of Civil and Environmental Engineering, Princeton University, Princeton, New Jersey, USA, [2]Department of Hydraulic Engineering, Tsinghua University, Beijing, China, [3]Department of Earth and Environmental Sciences, Brooklyn College, Brooklyn, New York, USA, [4]Department of Agronomy-Crops, Soils, Environmental Sciences and Department of Earth, Atmosphere and Planetary Sciences, Purdue University, West Lafayette, Indiana, USA

Abstract The objective of this study is to examine the structure and evolution of storms that produce flash floods in "small" urban watersheds. The study site is Harry's Brook, a 1.1 km^2 urban watershed in Princeton, New Jersey. A catalog of 15 storms is developed for Harry's Brook based on paired observations of streamflow and rainfall. Lagrangian analyses of storm properties are based on storm tracking procedures utilizing 3-D radar reflectivity observations from the KDIX (Fort Dix, New Jersey) Weather Surveillance Radar, 1988 Doppler. Analyses focus on the storm elements that were responsible for the peak rainfall rates over the watershed. The 22 July 2006 storm, which produced the record flood peak in the catalog (a unit discharge of 26.8 $m^3 s^{-1} km^{-2}$) was characterized by thunderstorm cells that produced more than 50 cloud-to-ground lightning strikes and "collapsed" over Harry's Brook. The 3 June 2006 storm, which produced the third largest flood peak (a unit discharge of 11.1 $m^3 s^{-1} km^{-2}$), was a "low-echo centroid" storm with no lightning. We use cloud-to-ground flash rate, echo top height, maximum reflectivity, and height of maximum reflectivity as key variables for characterizing convective intensity. Storm motion is examined through a time series of storm speed and direction. The 22 July 2006 and 3 June 2006 storms provide end-members of storm properties, centering on "convective intensity," which are associated with flash flooding in small urban watersheds. Extreme 1–15 min rainfall rates are produced by warm season convective systems at both ends of the convective intensity spectrum.

1. Introduction

Flash flooding in urban watersheds is among the most severe natural hazards in terms of economic loss and fatalities, the severity of which is projected to increase with rapid urbanization and with greenhouse gas driven climate change [*Intergovernmental Panel on Climate Change*, 2007; *Villarini et al*., 2009; *National Research Council*, 2012; *Yang et al*., 2013a, 2015]. The occurrence of flash floods is linked to both meteorological (e.g., storm-scale processes and synoptic environment) and hydrological processes (linked to impervious coverage, density of the drainage network, and basin topography) (see, e.g., *Davis* [2001], *Ntelekos et al*. [2006], and *Ogden et al*. [2011] for more details). Previous studies have extensively examined the synoptic and mesoscale environments of flash flood events [*Maddox et al*., 1979; *Schumacher and Johnson*, 2004; *Zipser et al*., 2006; *Houze et al*., 2011; *Peters and Schumacher*, 2014]. The storm-scale evolution of flash flood producing systems has received less attention [*Petersen et al*., 1999; *Smith et al*., 2005; *Ntelekos et al*., 2008] and will be the principal topic of this study.

The objective of this study is to investigate the structure and evolution of storms that produce flash flooding in "small" urban watersheds. Surface rain rate largely controls infiltration and runoff generation processes related to flood response in urban watersheds. Variability of rainfall rate at short time scales (1–30 min) plays a prominent role in flash flooding over small urban watersheds [e.g., *Syed et al*., 2003; *Berne et al*., 2004; *Smith et al*., 2005; *Yang et al*., 2011; *Ogden et al*., 2011; *Peleg and Morin*, 2012] and is closely tied to time-varying properties of storm elements. We will examine these properties from a Lagrangian perspective, following storms as they pass over the study watershed. Lagrangian analyses of storm properties are based on storm tracking procedures that utilize 3-D radar reflectivity observations from the KDIX (Fort Dix, New Jersey) Weather Surveillance Radar, 1988 Doppler (WSR-88D). These analyses focus on the storm elements that are responsible for the peak rainfall rates in the study watershed, as determined from a Joss-Waldvogel disdrometer. The storm properties that we examine are related to convective intensity, storm motion, and storm size. We use echo top height, maximum reflectivity in the cell, and cloud-to-ground lightning flash rate as the key variables for characterizing convective

intensity. Storm motion is examined through a time series of storm speed and direction. The time series of storm area are used to characterize a key element of storm structure.

Organized thunderstorm systems are dominant agents of flash flooding over urban regions of the United States east of the Rocky Mountains. In *Smith and Smith* [2015], analyses of U.S. Geological Survey discharge observations and NLDN cloud-to-ground lightning observations are used to show that more than 50% of urban flash floods in the U.S. east of the Rocky Mountains are due to thunderstorms.

In *Smith et al*. [2005], it is shown that record urban flooding in Baltimore on 13 June 2003 was associated with a collapsing thunderstorm cell. The storm had anomalously large values of echo top height, reflectivity, and cloud-to-ground lighting flash rate prior to producing extreme rain rates and record flooding over Baltimore. The links between convective downdrafts and extreme short-term rainfall rates have not been extensively explored. *Tattelman and Willis* [1985] suggest that the world record 1 min rainfall rate (as of 1985) of 1875 mm h^{-1} on 4 July 1956 in Unionville, Maryland, was linked to strong downdrafts [see also *Willis and Tattelman*, 1989]. The 4 July 1956 Unionville storm was embedded in a large convective outbreak that produced hail and tornados [*Engelbrecht and Brancato*, 1959].

Supercell thunderstorms, among the most convectively intense storms in the world, are responsible for some of the largest rainfall rates at short time intervals and extreme urban flooding, including the 5 May 1995 Dallas Hailstorm, which resulted in 17 casualties from flash flooding [*Smith et al*., 2001]. In sharp contrast, record flooding in Fort Collins, Colorado, on 28 July 1997 was produced by a "low-echo centroid" storm with virtually no lighting [*Petersen et al*., 1999]. Examining the role of convective intensity in producing extreme rainfall rates is one of the key objectives of this study (see, e.g., *Zipser and Lutz* [1994], *Holle and Bennett* [1997], and *Petersen and Rutledge* [1998] for the discussion of important issues linking convective intensity and rainfall rate).

Doswell et al. [1996] argue that storm speed is a key storm property for flash flooding. Rainfall at a location is the product of rainfall rate and duration, suggesting that slow-moving storms can be effective flood agents in many settings. In addition, *Davis* [2001] discussed the impacts of other key storm properties on flash flooding, including shape and orientation of storm cells, and storm motion relative to drainage network [see also *Doswell et al*., 1996; *Morin et al*., 2006; *Peleg and Morin*, 2012].

Our study site is Harry's Brook, a 1.1 km^2 urban watershed in Princeton, New Jersey, which is an exceptionally "flashy" watershed, based on the frequency of flood peaks exceeding a unit discharge of 1 $m^3 s^{-1} km^{-2}$ [*Smith and Smith*, 2015; L. Yang et al., Flash flooding in small urban watersheds: rainfall variability and storm event hydrologic response, under revision to *Water Resource Research*, 2015b, hereinafter referred to as Yang et al., under revision manuscript, 2015b]. We have carried out field experiments in Harry's Brook since 2005, with a focus on the impact of land surface properties and rainfall variability on flood response. It is an interesting setting for examining the properties of flash flood producing storms, because of its "end-member" flash flood hydrology and for the exceptional observational resources that are available. A catalog of 15 storms is developed for Harry's Brook based on paired observations of streamflow and rainfall.

The paper is organized as follows. In section 2, we describe the physical setting of the Harry's Brook watershed and introduce the storm catalog that is used for hydrometeorological analyses. A brief introduction to the storm tracking algorithm is also provided in this section. Results are presented in section 3, focusing on detailed case studies of two severe flash flooding storms (section 3.1) and composite analyses of all storms in the catalog (section 3.2). In section 3.3, connections between lightning frequency and extreme rainfall rates are presented. A summary and conclusions are given in section 4.

2. Data and Methodology

2.1. Study Watershed and Storm Catalog

Harry's Brook drains the urban core of Princeton, New Jersey, and our analyses focus on the most densely urbanized portion of the watershed (see the insert map in Figure 1). The drainage area of Harry's Brook above the Harrison Road stream gaging station (Figure 1) is 1.1 km^2.

We develop a catalog of warm-season (May to October; see Table 1) convective systems that passed over Harry's Brook from 2005 to 2006, corresponding to the period of stream gaging in Harry's Brook. The selection

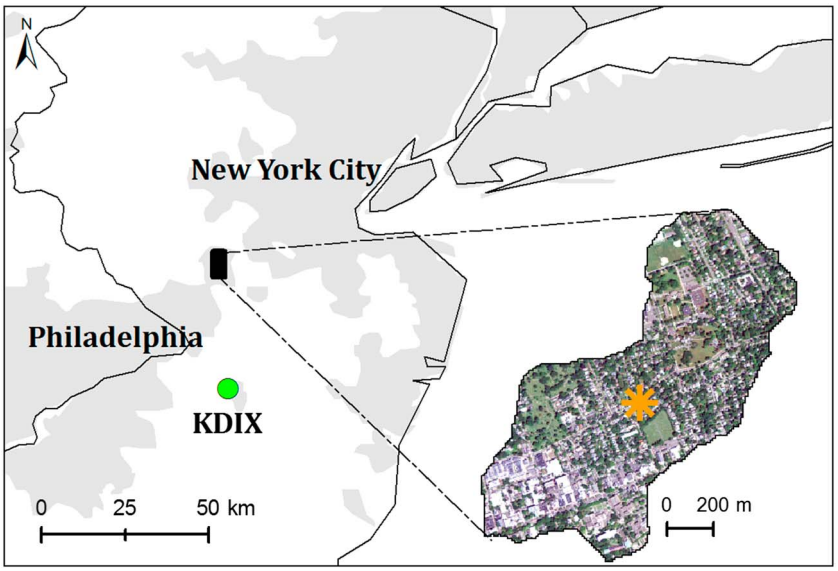

Figure 1. Location of the Harry's Brook in the northeastern U.S. The green circle represent the location of the WSR-88D radar in Fort Dix, New Jersey. The shaded area represents the urban coverage of the northeastern U.S. The insert map shows the Harry's Brook watershed in Princeton, New Jersey. The orange star in the map highlights the location of the Joss-Waldvogel disdrometer.

of flash flood producing storms is based both on the magnitudes of associated flood peaks and on surface rain rates. Surface rain rate is obtained from raindrop size distribution measurements using a Joss-Waldvogel disdrometer, with a temporal resolution of 1 min (see *Smith et al.* [2009] for details) (see Figure 1 for location). Rainfall observations from the disdrometer agreed well with two collocated accumulation rain gauges (Yang et al., under revision manuscript, 2015b). Fifteen storms were selected for analysis. All of these storms (except the 29 June 2005 case) occur within a time window from late afternoon to early evening, reflecting the warm season diurnal climatology of flash flood producing storms in the northeastern U.S. (see *Ntelekos et al.* [2007], *Zhang et al.* [2009], and *Yeung et al.* [2011, 2015] for more details). Flood peaks produced by the storms in the catalog exceed a unit discharge of 1 $m^3 s^{-1} km^{-2}$ (unit discharge is flood peak discharge divided by drainage area). The correlation between flood peak discharge and maximum 1 min rainfall rate is 0.66 and is 0.89 for maximum 30 min rainfall rate (see Yang et al., under revision manuscript, 2015b for detailed rainfall

Table 1. Overview of the Storm Catalog Over the Harry's Brook Watershed (CG Lightning Flashes Are Counted Within a 60 Minute Period and 10 km Radius Centered at the Location of the Disdrometer)

Year	Date	Rain Peak Time (HHMM)	Max 1 min Fainfall Rate (mm h^{-1})	Max 15 min Rainfall Rate (mm h^{-1})	Number of CG Lightning Flashes in 60 min Period	Magnitude of Flood Peak Discharge ($m^3 s^{-1} km^{-2}$)
2005	29 Jun	1938	78	55	5	17.8
	2 Jul	0546	93	50	17	9.5
	15 Aug	0302	66	37	0	7.8
2006	12 May	0345	57	21	0	2.5
	16 May	0043	83	26	1	1.0
	3 Jun	0021	115	51	0	11.1
	3 Jun	0359	81	49	3	8.9
	8 Jun	2318	60	35	0	2.8
	14 Jun	2327	64	36	0	4.1
	23 Jun	2314	63	32	11	2.5
	30 Jun	0246	36	17	30	1.1
	13 Jul	0234	107	38	55	4.8
	22 Jul	0006	88	61	55	10.3
	22 Jul	2047	120	78	50	26.8
	5 Oct	0401	123	66	11	10.3

runoff analyses). The largest flood peak occurred during the late afternoon on 22 July 2006, with a unit peak discharge of 26.8 $m^3 s^{-1} km^{-2}$. This flood peak magnitude of the 22 July 2006 storm is comparable to the largest observed unit discharge flood peaks for the eastern U.S. [*Smith et al*., 2005]. The flood peak occurred within 11 min of the peak rain rate for the event (see Yang et al., under revision manuscript, 2015b, for detailed analyses of extraordinary flood response). The frequency of flood peaks exceeding 1 $m^3 s^{-1} km^{-2}$ in Harry's Brook (Yang et al., under revision manuscript, 2015b) is comparable to the flashiest watersheds in the contiguous U.S. [*Smith and Smith*, 2015].

2.2. Storm Tracking Algorithm

We utilize the TITAN (Thunderstorm Identification, Tracking and Nowcasting) [see *Dixon and Wiener*, 1993] storm tracking algorithms to examine the Lagrangian properties of each storm event in the catalog (see, e.g. *Smith et al*. [2001], *Javier et al*. [2007], and *Yang et al*. [2013b] for more details about the algorithm). Storm-tracking analyses are based on 3-D reflectivity fields obtained from the KDIX (Fort Dix, New Jersey) WSR-88D (Weather Surveillance Radar, 1988 Doppler) (see the location in Figure 1). The radar reflectivity data have been subjected to quality control procedures used in previous studies [e.g., *Smith et al*., 2010, 2012; *Wright et al*., 2012]. Time-varying properties for each storm element are derived as a part of the identification and tracking procedures. The variables analyzed in this study include the area of storm elements (projected area of storm envelope when viewed from above), maximum reflectivity, echo top height, storm speed, and storm direction.

We use a 40 dBZ reflectivity threshold and a 50 km^3 volume threshold to identify storm elements for each event in the storm catalog. The 40 dBZ threshold has been used in previous studies to select convective events [*Steiner et al*., 1995; *Schumacher and Johnson*, 2004; *Zipser et al*., 2006; *Rasmussen et al*., 2014]. A contiguous region of reflectivity values exceeding 40 dBZ is identified as a storm cell provided that the total volume with reflectivity exceeding 40 dBZ is also greater than 50 km^3. Echo top height for each storm element is defined as the maximum height of radar reflectivity exceeding 18 dBZ (equal approximately to a rain rate of 0.2 mm h^{-1}). We will use the term "storm element" for the features tracked using the 40 dBZ and 50 km^3 thresholds. The tracked storm elements are typically storm cells or multiple cells within a convective system.

For each storm event, we picked "dominant simple tracks," which consist of simple-track storm elements that pass through Harry's Brook but have no splits or mergers with other storm elements [e.g., *Yang et al*., 2013b; *Yeung et al*., 2015]. Other storm tracks were discarded even though they are embedded within the same convective system. Since the spatial scale of Harry's Brook is comparable to the average storm cell size, it is assumed that only one storm element contributes to the peak rain rate in the watershed.

3. Results and Discussion

3.1. Case Studies: 22 July 2006 and 3 June 2006

The 22 July 2006 storm, as noted above, produced the largest flood peak in Harry's Brook during the observation period (2005–2006). The 3 June 2006 storm produced the third largest flood peak in our catalog (a unit discharge of 11.1 $m^3 s^{-1} km^{-2}$). The peak 1 min rain rate for the 3 June 2006 storm (115 mm h^{-1}) is comparable to the peak 1 min rain rate for the 22 July 2006 storm (120 mm h^{-1}; Figure 2); the maximum 15 min rain rate for the 22 July storm is 78 mm h^{-1} and for the 3 June storm is 51 mm h^{-1}. Correlation analyses between peak rainfall rate, averaged over time intervals ranging from 1 to 60 min, and peak discharge show that rainfall variability on time scales from 5 to 15 min rain are most important for flood peak magnitudes in Harry's Brook (see Yang et al., under revision manuscript, 2015b, for more details).

The 22 July 2006 storm, like many urban flash floods in the eastern U.S., was associated with an approaching upper level trough and passage of a surface cold front (see daily weather map available at http://www.wpc.ncep.noaa.gov/dailywxmap/index_20060722.html) [see, e.g., *Schumacher and Johnson*, 2004; *Ntelekos et al*., 2008]. A cluster of convective cells developed in the warm sector east of the cold front. The peak hourly rainfall rate over Harry's Brook of 30 mm occurred from 2000 UTC to 2100 UTC (Figure 3a). The 22 July 2006 case can be categorized as cellular convection in broken lines, following the storm classification schemes developed by *Gallus et al*. [2008]. The motion vector (based on the tracking algorithm TITAN) for the 22 July storm is around 70°NNE (zero is toward true north; see Figure 3a for the vector of dominant

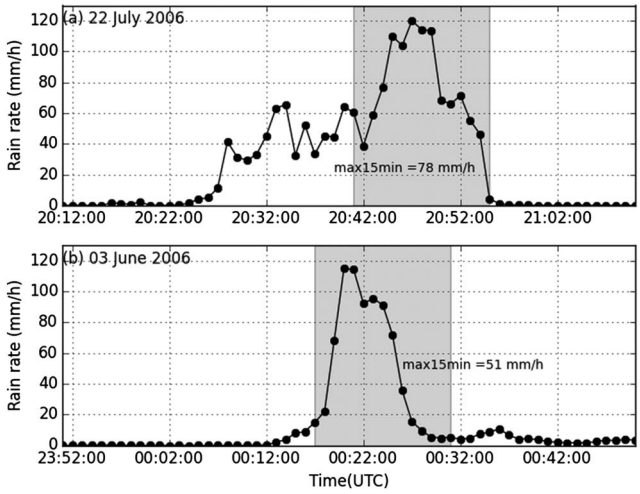

Figure 2. Times series of 1 min rain rate for (a) 22 July 2006 and (b) 3 June 2006 storm (based on observations from the Joss-Waldvogel disdrometer; see Figure 1 for location). The shaded area denotes the temporal span of the maximum 15 min rain rate.

propagation), almost parallel with the steering level winds, and computed as the mean wind between 850 hPa and 500 hPa.

The 3 June 2006 storm, like the 22 July 2006 storm, was associated with an approaching trough and the passage of a cold front (see daily weather map available at http://www.wpc.ncep.noaa.gov/dailywxmap/index_20060603.html). The storms that produced flash flooding in Harry's Brook formed along a developing warm front in New Jersey. The motion of the 3 June 2006 storm was to the right of steering level winds and reflects the influence of the frontal boundary in dictating storm evolution (Figure 3b).

The most striking contrasts between the 22 July and 3 June storms center on the "convective intensity." The 22 July storm had peak echo top heights of over 11 km preceding and during the period of peak rainfall rates over Harry's Brook (Figure 4b). By contrast, the peak echo tops for the 3 June storm fluctuate between 6 km and 7 km during and after peak rainfall over Harry's Brook (Figure 4b). The 3 June 2006 storm exhibited a low-echo centroid (LEC) structure (compare Figures 5–7) which has been associated with flash floods in other settings, notably the 28 July 1997 Fort Collins flash flood [*Petersen et al*., 1999]. Like the Fort Collins storm, the 3 June storm produced no cloud-to-ground lightning. By contrast, the 22 July storm produced extensive lightning, especially as it passed over Harry's Brook.

The analyses in Figure 4 are based on tracked storm elements for the two storm events and are referenced to a time origin which corresponds to the peak rainfall rate over Harry's Brook. Storm area for the tracked storm elements for both the 22 July and 3 June storms fluctuate between 100 km^2 and 150 km^2 around the period

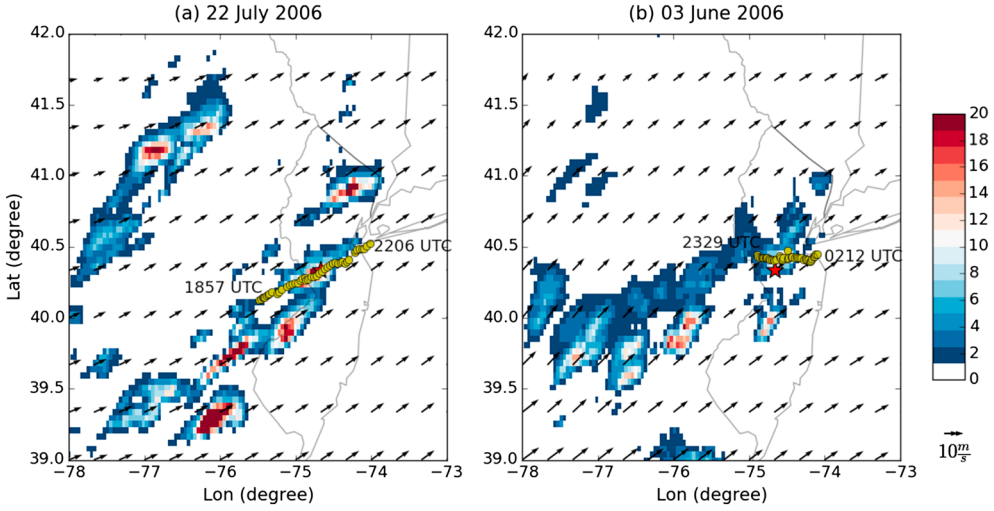

Figure 3. Wind fields and storm tracks for the (a) 22 July 2006 and (b) 3 June 2006 storm. Grey lines denote the state boundaries of New Jersey and New York. Black arrows represent the average wind fields (based on the North American Regional Reanalysis data; see *Mesinger et al*. [2006]) between 850 hPa and 500 hPa during the peak rain rate hour; shaded color is hourly accumulated rainfall (mm; based on National Centers for Environmental Prediction stage IV data set; see *Lin and Mitchell* [2005]) at the peak hour. Red stars represent the location of Harry's Brook watershed. Yellow dots represent the dominant simple track of storm cells, tracked between two time periods as indicated on the map.

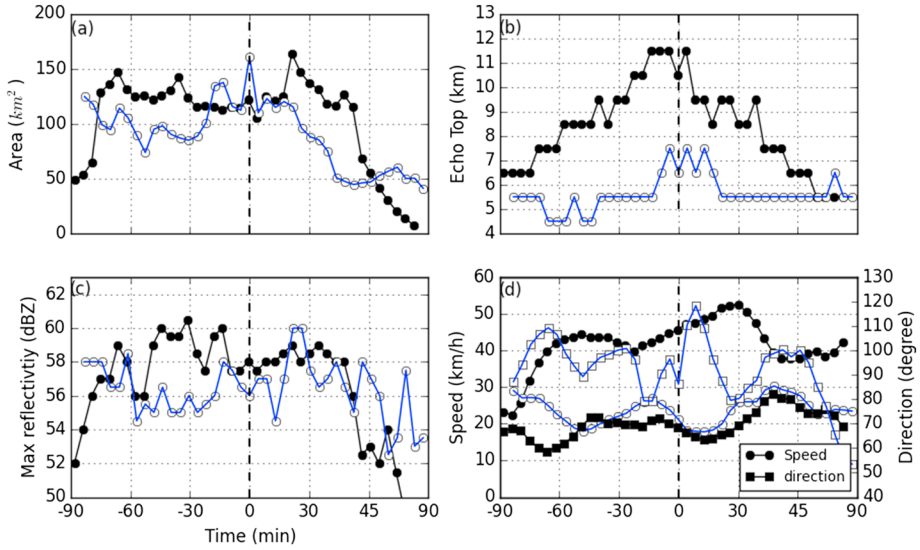

Figure 4. Time series of (a) area of storm cells, (b) echo top height, (c) maximum reflectivity, and (d) speed and direction of storm cells for 22 July 2006 (black line with closed symbols) and 3 June 2006 (blue lines with open symbols). The *x* axis represents referenced time relative to the occurrence of peak rain rate for each storm event; the value of zero is the time when peak rain rate occurs.

of peak rainfall rate (Figure 4a). Maximum reflectivity is greater than 54 dBZ for more than 2 h for both storms. The largest values of reflectivity for the 22 July storm exceed 60 dBZ and are concentrated in the period before peak rainfall rate. Maximum reflectivity values for the 3 June storm are generally less than those for the 22 July storm, but there is a sharp increase in maximum reflectivity to 60 dBZ that begins 20 min after the storm passes over Harry's Brook. Reflectivity values for the 3 June storm are large for low-echo centroid storms [*Petersen et al*., 1999], in which the relatively small concentration of mixed phase hydrometeors typically results in markedly lower reflectivity values than in storms with hail and graupel. The large low-level reflectivity values in LEC storms are consistent with the large rainfall rates that occurred on 3 June.

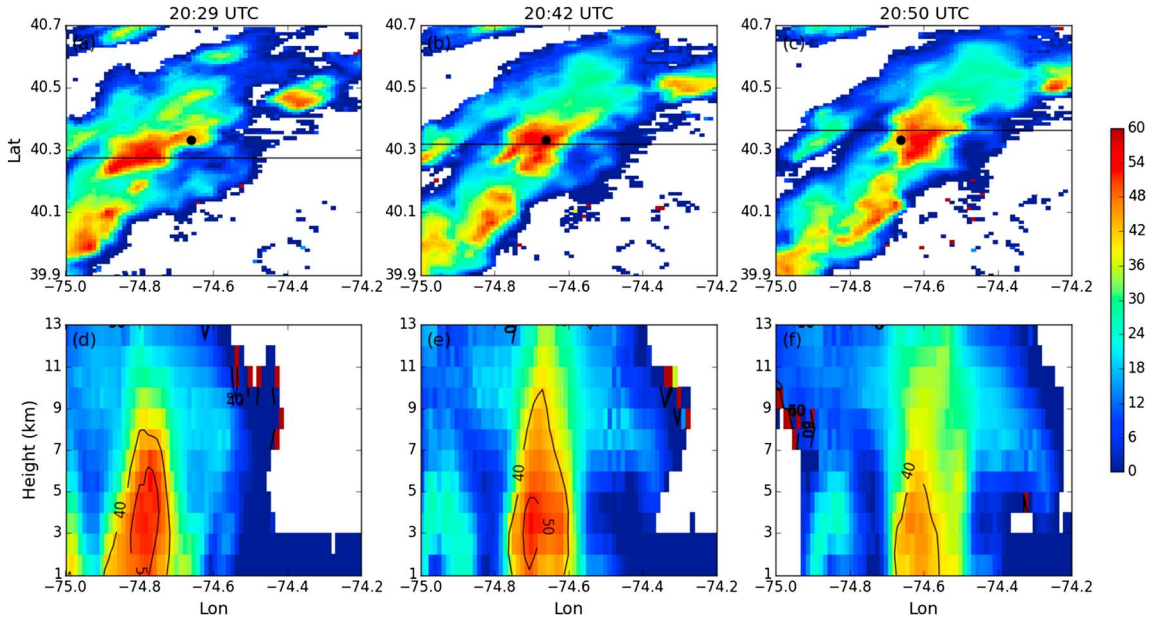

Figure 5. Reflectivity of the 22 July 2006 storm at (a) 2029 UTC, (b) 2042 UTC, and (c) 2050 UTC on the height of 4 km (Cartesian plan view); black lines cross the centroids of storms (determined by TITAN) at each time period; (d, e, and f) Vertical cross sections along the black lines shown in Figures 5a–5c, respectively. The shaded color denotes radar reflectivity (dBZ). Black curves in Figures 5d–5f denote contours of 40 dBZ and 50 dBZ, respectively. The black dots represent the location of Harry's Brook watershed.

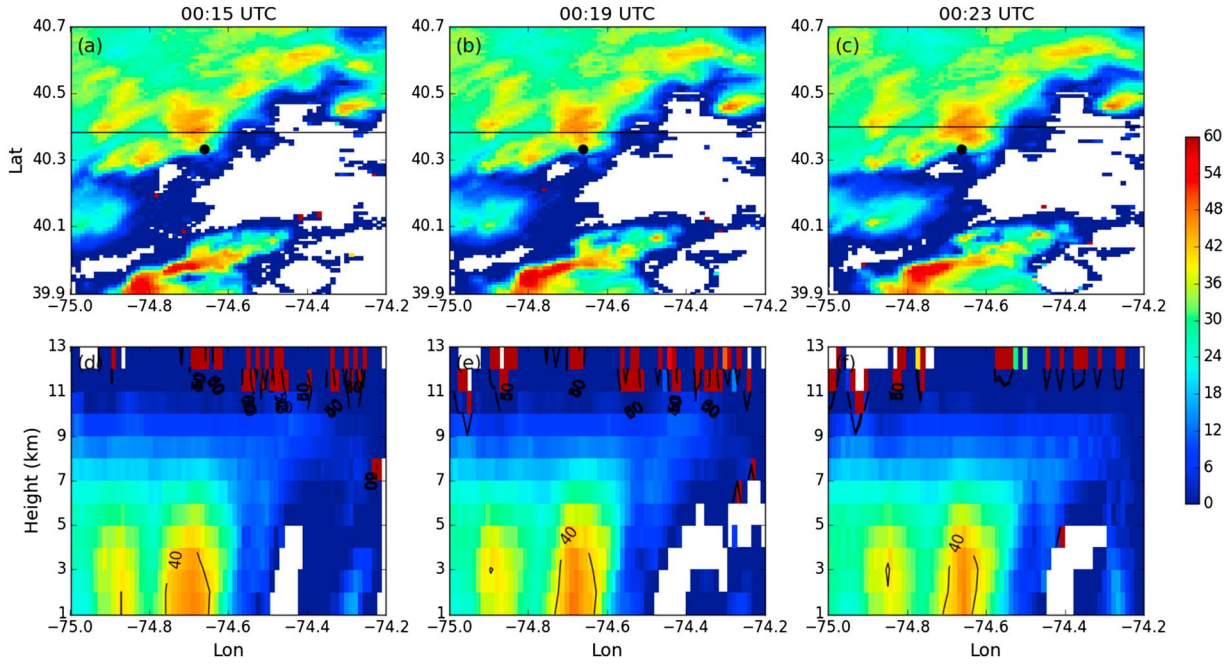

Figure 6. Same as Figure 5 but for 3 June 2006 storm at (a) 0015 UTC, (b) 0019 UTC, and (c) 0023 UTC on the height of 4 km (Cartesian plan view); (d, e, and f) Vertical cross sections along the black lines shown in Figures 6a–6c, respectively.

The 22 July storm exhibits striking growth in convective intensity, as reflected in the time series of echo top height (Figure 4b), during the period before it passes over Harry's Brook and a sharp decrease in convective intensity after it passes over Harry's Brook. This form of storm evolution is consistent with the "collapsing" storm cell evolution that produced record urban flooding in Baltimore [*Smith et al.*, 2005] (see also *Goodman et al.* [1988] for examples of extreme rainfall and collapsing convective cells). The evolution of the 22 July storm suggests that collapse of storm cells can be an important feature for heavy rainfall rates at the surface for Harry's Brook. The 3 June 2006 storm exhibits growth in echo top height from a steady 5.5 km to 6–7 km elevation in the 15 min before peak rainfall rate and a decrease in echo top height back to the steady 5.5 km 20 min after peak rainfall rate.

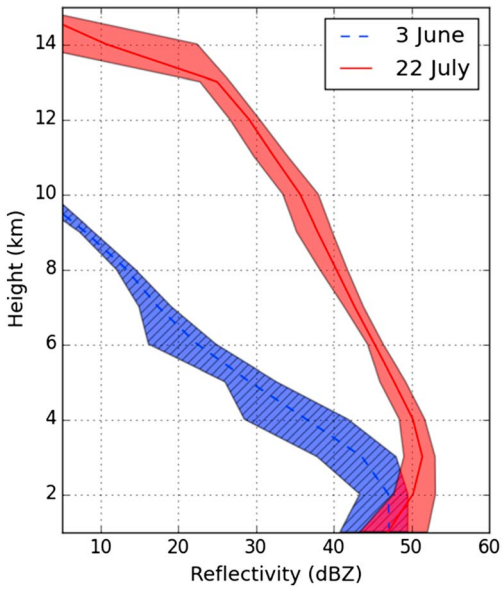

Figure 7. Composite vertical structures of storm cells over Harry's Brook watershed at peak rain rate time: 3 June (blue hatched) and 22 July 2006 (red solid). Solid (dash) lines represent mean vertical profiles of storm structures for 22 July (3 June) 2006. The observed range of radar reflectivity is shaded.

The storm motion for the 3 June storm is slower than for the 22 July storm (Figure 4d). Storm speed (estimated as the mean speed of storm cells) for the 22 July storm averages 45 km h^{-1} during the 40 min period centered on the peak rainfall rate, more than twice the 20 km h^{-1} for the 3 June storm. Storm speed for the 22 July storm is increasing as it passes over Harry's Brook, in contrast to the slowing storm motion for the 3 June storm. As noted above, the 22 July storm motion is aligned with the 850 to 500 hPa steering winds, while the 3 June storm motion is to the east of the steering winds. Slow storm motion can be an important element of flash flooding [*Doswell et al.*, 1996].

We compared the vertical structures of the 22 July 2006 storm (Figure 5) with the 3 June 2006 storm (Figure 6) at the time of peak rain rate. The 3 June 2006 storm

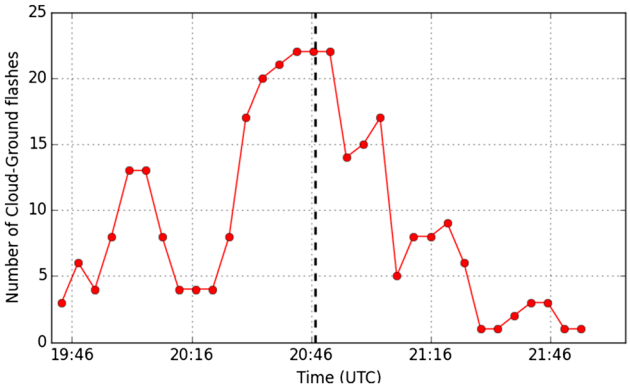

Figure 8. Time series of cloud-to-ground lightning flash counts for the 22 July 2006 storm. Cloud-to-ground flashes are counted within radius of 10 km centered at the locations of storm cell centroid.

exhibits low-echo centroid structure, with an echo top height around 5–7 km, in contrast with a 14 km echo top for the 22 July 2006 storm. Figure 7 presents the composite vertical structures of both storms over the Harry's Brook watershed at the time when peak rain rates are observed. Both events have comparable surface reflectivity (around 50 dBZ). However, the reflectivity drops sharply with height for the 3 June storm (mean reflectivity drops below 40 dBZ at the height of 3–4 km), in contrast to the profile for the 22 July storm.

We utilized cloud-to-ground (CG) lightning observations to further examine the differences between the 22 July 2006 storm and the 3 June 2006 storm. CG lightning data are obtained from the National Lightning Detection Network (NLDN) (see *Orville and Huffines* [2001] for more details). During the hour of peak rainfall (2000 UTC to 2100 UTC), 50 cloud-to-ground (CG) lightning flashes were observed for the 22 July 2006 storm over the region within a radius of 10 km centered over Harry's Brook (Table 1). There was no CG lighting observed for the 3 June 2006 storm (Table 1). For the 22 July storm, the time series of CG flashes within 10 km of the tracked storm centroid (Figure 8) illustrate the striking growth in convective intensity during the 30 min preceding peak rainfall rate and the precipitous decrease in convective intensity following the peak rainfall rate over Harry's Brook. The decrease of CG lightning frequency corresponds to the decrease of echo top height and maximum reflectivity, providing further evidence for the importance of dissipating storm cells for extreme rainfall and flash flooding. Most of the CG lighting flashes contain multiple strokes (four to five strokes per flash on average). Multi-stroke flashes are associated with complex spatial distribution of charge within storms that are experiencing mature or decaying phases [*Krehbiel*, 1986].

3.2. Composite Analyses for All Storms

We examine the structure and evolution of flash flood producing storm properties based on analyses of all storms in the catalog, focusing on the relative importance of the features identified from analyses on 22 July and 3 June 2006 storms (in terms of storm evolution and structure). As shown in Figure 9 (similar to Figure 4 but for all storm events), four variables were derived for each storm event based on storm tracking analyses. Each dot in the figure represents an individual storm element that is included in dominant simple tracks (time 0 for each plot is the time of peak rain rate). We observed a sharp drop of storm area, echo top height, maximum reflectivity, and storm speed within a 2 h time window (within the life cycles of all storm events). Average maximum reflectivity is approximately 60 dBZ at the time of the peak rainfall rate and drops to 50 dBZ within 60 min following peak rain rates. Echo top height decreases by 5 km, from around approximately 11 km to 6 km (Figure 9b). Decreasing values of maximum reflectivity and echo top height point to the role of dissipating storm cells described in producing peak rainfall rates. Storm area also tends to decrease following peak rain rate (Figure 9a). Storm motion tends to slow following the peak rain rate period (Figure 9d). Slow storm movement provides a favorable environment for flash flooding events from the perspective of a larger spatial scale [*Chappell*, 1986; *Doswell et al*., 1996].

The evolution of storm features over the life cycle of the storm element (as in Figure 9) provides important insight to extreme rainfall from flash flood producing storms. Special attention, however, should also be paid to behavior of storm elements as they produce peak rain rates. We used a smaller time window (30 min centered over the time of peak rain rate) for the following analyses. Table 2 summarizes the properties of storm cells at the time of peak rain rates for all storm events in the catalog. The median value of maximum reflectivity is 58 dBZ and the 10th and 90th percentiles of maximum reflectivity are 55 dBZ and 63 dBZ, respectively. The median value of echo top height, 8.5 km, is 3 km higher than the 10th percentile. The 90th percentile of echo top height 10.2 km is only 1.7 km larger than the median value. The spread in values of echo top height reflects the division of storm events between convectively intense storms and storms

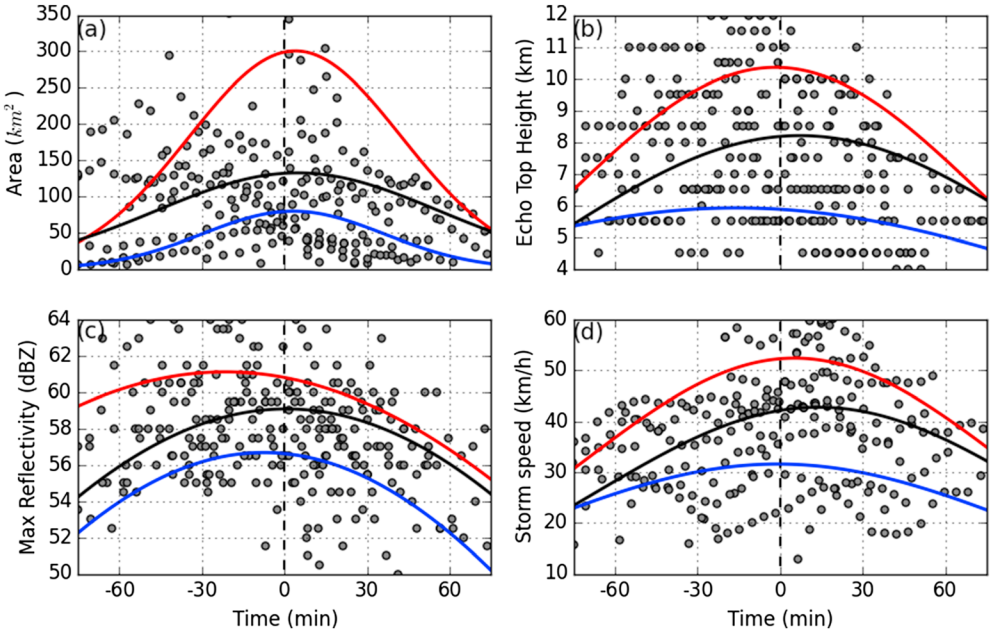

Figure 9. Ensemble properties for all storms: (a) area of storm cells, (b) echo top height, (c) maximum reflectivity, and (d) storm speed. Red and blue curves represent the 75th and 25th percentile for all storm properties, respectively. Black curves represent the median values. Grey dots represent observations from storm cells within the catalog. Each dot represents a storm element. Time is centered on peak rain rates.

exhibiting low-echo centroid structure. The mean size of storm cells is greater than 100 km^2, with large variability among different storm events. The dominant direction of storm movement is toward the northeast (75° from due North), like the movement for the 22 July 2006 storm.

Figure 10 shows the normalized rates of change of storm variables within the 30 min time window (centered over the time of peak rain rate). The normalized change rate takes the form as

$$C(X) = {}^{d}N_X/_{d}t,\ N_X = (X_t - \mu_X)/\sigma_X \quad (1)$$

where X represents each variable, t is time, and μ and σ represent the mean value and standard deviation of each variable within 30 min time window (centered over the time of peak rain rates), respectively. The direction of storm motion was first decomposed into zonal (u) and meridional (v) components. The mean direction of storm motion was based on synthetizing the averaged u and v component, respectively. We note that the mean direction ranges from 0° to 120° for all storm elements that pass over Harry's Brook.

Echo top height, maximum reflectivity, and storm area generally show decreases over the 30 min time window centered on peak rainfall rate. Decreases in the height of the echo top and maximum reflectivity are linked to the dissipation of storm cells. This feature is consistent with the findings over the entire life cycle of storms (Figure 9). Storm speed generally increases and storm motion veers to a more northerly direction.

Table 2. Structural Properties of Storm Cells Producing Peak Rain Rates[a]

			Percentiles				
Variables	μ	σ	10th	25th	50th	75th	90th
Max reflectivity (dBZ)	59	3.2	55	57	58	60	63
Height of max reflectivity (km)	2.7	1.0	1.5	2.0	3.0	3.5	4.1
Height of echo top (km)	7.8	1.9	5.5	5.8	8.5	9.6	10.2
Area (km^2)	161	189	41	61	84	157	452
Storm speed (km h^{-1})	43.0	11.8	13.8	31.0	42.5	47.3	60
Storm direction (degrees)	75	20.5	25	56	65	97	101

[a] μ and σ represent mean value and standard deviation for all storms in the catalog (Table 1).

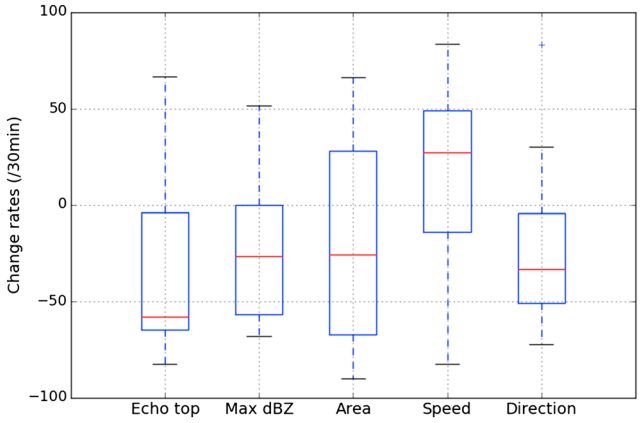

Figure 10. Rates of change for variables related to structural properties of storms within 30 min time window centered at the time of peak rain rates. The box spans the 25th and 75th percentiles, and the whiskers represent the minimum and maximum values. The red lines in the box represent the median values. Blue star highlights the outliers.

The accelerated storm motion suggests a downwind (relative to the steering-level wind) or "forward" propagation of storm cells, which is closely tied to the interactions of storm outflows (i.e., gust front, due to the downdrafts of collapsing storm cells) with ambient convective environment favorable for forward initiation of new storm elements (see, e.g., *Corfidi* [2003] for more discussion). The northward shift of storm motion is determined jointly by the steering-level wind vector and storm propagation vector, with the latter pointing toward north relative to steering-level wind.

The contrasting properties of the 22 July 2006 storm and 3 June 2006 storm, which were examined in section 3.1, are broadly reflected in the larger sample of all storms. The 14 June and 23 June 2006 storms share the same contrasts in terms of vertical structure as the 22 July and 3 June 2006 storms. The 14 June and 23 June 2006 storms have comparable surface rainfall rates at both maximum 1 min (64 mm h^{-1} and 63 mm h^{-1}, respectively) and 15 min (36 mm h^{-1} and 32 mm h^{-1}, respectively) time scale. However, the mean echo top height (average of all storm cells within 30 min time window centered on over the time of peak rain rate) for the 14 June storm is no more than 5 km, in contrast with the 23 June storm with mean echo top height of about 11 km (figure not shown).

Based on case studies in section 3.1 and composite analyses in this section, we found general features of storm evolution for flash flood producing storms. However, storms in the catalog, as represented by 22 July and 3 June storms can vary significantly in storm structure, providing end member of storm properties associated with flash flooding in small urban watersheds.

3.3. Lightning, Convective Intensity, and Surface Rain Rates

We found strong correlations between CG lightning frequency, echo top height, and height of maximum reflectivity (Figure 11) for events in the storm catalog, supporting the use of CG lightning frequency as an indicator of convective intensity within our catalog of storms. In Figure 11 we show scatterplots of CG lightning frequency (number of CG lightning flashes within 60 min period) with echo top height, height of maximum reflectivity, maximum 1 min, and maximum 30 min rain rates at the surface. The statistics of all the variables are based on a 60 min time window (when the peak surface rain rate is observed for each storm event). Echo top height and height of maximum reflectivity are the mean values for all storm cells within the 60 min time window.

There are not strong relationships between CG lightning frequency and rainfall rate, either at the 1 min or 30 min time scale. The 3 June 2006 storm produced a peak rain rate of 115 mm h^{-1} (denoted as blue dot in Figure 11), but there are no CG lightning flashes observed during the 60 min time window (the 22 July 2006 storm produced 50 CG lightning flashes with a peak rain rate of 120 mm h^{-1}, denoted as red dot in Figure 11). In addition, the 3 June 2006 storm is much lower in both mean echo top height and height of maximum reflectivity, compared to the 22 July 2006 storm (Figures 11a and 11b). The mean echo top height is around 5 km for the 3 June 2006 storm (also see Figure 11a). If, however, we restrict attention to those events with large CG lightning frequencies in the catalog, we find large surface rain rates at 1–30 min time scale (Table. 1). The storms with the three highest lightning strike rates (more than 50 flashes, 13 July 2006, 0006 UTC 22 July, and 2047 UTC 22 July 2006) produced peak rain rates of 107 mm h^{-1}, 88 mm h^{-1}, and 120 mm h^{-1}, respectively. Storms with large CG lightning rates are those with relatively high echo tops (Figure 11b). The top seven storms (in terms of echo top height) produced the largest CG lightning frequencies (30 strikes per event on average). Storms with smaller CG lightning frequencies (less than five strikes per event) are characterized with low-echo centroids (i.e., echo top height around 5 km). Although there is no

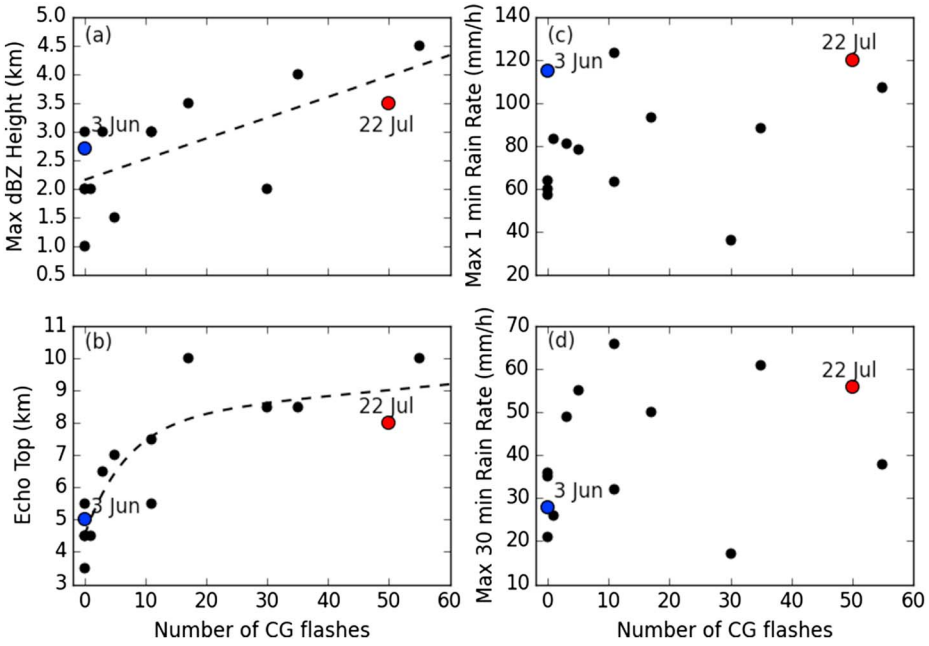

Figure 11. Correlation between cloud-to-ground lightning frequency (number of CG flashes within 60 min period) with (a) height of maximum reflectivity (mean), (b) echo top height (mean), (c) maximum 1 min rainfall rate, and (d) maximum 30 min rainfall rate. Dashed lines in Figures 11a and 11b denotes relationships between height of maximum reflectivity/ echo top height and CG frequency, respectively. Red and blue dots denote the 22 July 2006 storm and 3 June 2006 storm, respectively.

direct relationship between CG lightning flash density and rainfall rate, the likelihood of extreme rainfall rates is related to lightning flash density (see *Tapia et al.* [1998] for related analyses).

The relationship between convective intensity and extreme rain rates has been debated in previous studies. Severe thunderstorms have been discounted as heavy rainfall producers based on arguments revolving around low precipitation efficiency. *Cotton and Anthes* [1989], for example, note that "storms producing the largest hailstones occur in strongly sheared environments; thus, in general, we should not expect that the storm systems producing the largest hailstones are also heavy rain producing storms." *Hamada et al.* [2015] recently examined the connection between extreme rainfall events and events with intense convection, based on spaceborne precipitation radar over tropical and subtropical regions, and found that the heaviest rainfall events are not generally associated with the most intense convection, even in regions where severe convective storms are representative of extreme weather events (see, e.g., *Zipser et al.* [2006] for related analyses). In contrast, *Smith et al.* [2001] have shown that supercell thunderstorms are important agents of extreme rainfall rate and flash flooding, especially in small urban watersheds, and *Smith et al.* [2011] have shown that some of the largest rainfall rates in the U.S. at time intervals less than 6 h (and flash floods) are associated with organized thunderstorms.

Based on the general examination of storm properties, we found that flash flood producing storms in our catalog are a mixture of events dominated by intense convection and events dominated by warm rain processes and exhibiting low-echo centroid structures. There are common features to these two types of flash flood producing storms, including a prevalence of collapsing storm cells in both groups. Flash flooding in small urban watersheds is closely linked to rainfall rate variability at time scales less than 30 min. Future studies will assess the "microstructure" of rainfall rate at these time scales, focusing on contrasts between intense convection and low-echo centroid storms.

4. Summary and Conclusions

Empirical analyses of the structure and evolution of flash flood producing storms were performed using rainfall rate observations from a disdrometer, 3 days WSR-88D reflectivity fields, and cloud-to-ground lightning

observations. The TITAN storm tracking algorithm was used to examine Lagrangian properties of storms that are responsible for peak rain rates at the surface. Storm properties were characterized through analyses of two contrasting storms that both produced extreme short-term rainfall rates and urban flash flooding. These results were further generalized through analyses of a larger sample of flash flood producing storms over Harry's Brook watershed. The main conclusions of this study are summarized below.

We developed a catalog of flash flood producing storms based on 1 min surface rain rate and streamflow observations over the Harry's Brook watershed in Princeton, New Jersey. Flood peaks produced by the storms in the catalog exceed a unit discharge of 1 $m^3 s^{-1} km^{-2}$. The largest flood peak occurred on 22 July 2006, with a peak unit discharge of 26.8 $m^3 s^{-1} km^{-2}$. The 3 June 2006 storm produced the third largest flood peak over Harry's Brook during the 2 year observing period.

The 22 July 2006 and 3 June 2006 storms provide end members of storm properties, centering on convective intensity, which are associated with flash flooding in small urban watersheds. Extreme 1–15 min rainfall rates are produced by warm season convective systems at both ends of the convective intensity spectrum. The 22 July 2006 storm is characterized by strong convection (as represented by heights of echo top and maximum reflectivity) and frequent cloud-to-ground lightning flashes within a 60 min rainfall period. Peak rain rate was observed during the transition stage from increasing to decreasing convective intensity, characterized by rapid decrease in echo top height and cloud-to-ground lightning frequency. The 22 July 2006 storm contrasts with the 3 June 2006 storm, which produced the third largest flood peak in the catalog (a unit discharge of 11.1 $m^3 s^{-1} km^{-2}$). The 3 June 2006 storm exhibited low-echo centroid and produced no CG lightning during the entire storm period.

Structure and evolution of flash flood producing storms were generalized through Lagrangian analyses of the 15 storms in the catalog. Peak rain rates are generally accompanied by decreases of echo top height, maximum reflectivity, and area of storm cells. Collapsing storm elements, as in the 22 July 2006 storm, are a common feature of flash flood producing storms (Figures 9 and 10). Movement of storm cells tends to slow following the period of peak rain rates. Future studies will examine the role of evolution and structural properties of flash flooding storms in determining microstructure of extreme rain rate (e.g., drop size distribution and drop arrival rate). Microstructures of rain rate are closely tied to rainfall variability at smaller temporal scale and play a prominent role in infiltration and runoff generation processes during flash flooding events over small urban watersheds and will be focused in future studies.

Cloud-to-ground lightning frequency is strongly correlated with convective variables including heights of echo top and maximum reflectivity. We did not find significant correlation between CG lightning frequency and rain rates for the entire storm sample. However, we note that maximum 1 min rain rate tends to increase with CG lightning frequency among storms with relatively large CG lightning frequencies (high-echo-top storms). Contrasting properties of convective intensity point to a spectrum of storms that produce urban flash floods. Examination of CG lightning frequency provides important insights to the dependence of rainfall intensity on convection and the relationship of rainfall intensity with structural properties of flash flooding storms.

Although we note that storm samples within the 2 year observing period are sufficient for meaningful conclusions, generalization should be made with caution. More storm samples with paired high-resolution surface rainfall observations and 3-D coverage of radar reflectivity need to be investigated. The analytical framework developed over Harry's Brook can be usefully transferred to other small urban watersheds with contrasting synoptic environment and land surface properties.

Acknowledgments

We thank three anonymous reviewers for their useful comments which improved the manuscript. This study was supported by the National Science Foundation (CDSE 1250232, AGS 1522 494, AGS 0847472, CBET-1058027, CBET-1444758, and AGS-1522492). L.Y. is also supported by China postdoctoral Science Foundation funded project (2015 M570110). NLDN data are provided by NASA Lightning Imaging Sensor (LIS) instrument team and LIS data center via Global Hydrology Resource Center (GHRC) located at the Global Hydrology and Climate Center (GHCC), Huntsville, Alabama, through a license agreement with Global Atmospherics, Inc. (now Vaisala). The data available from the GHRC are restricted to LIS science team collaborators and to NASA EOS and TRMM investigators. Detailed storm tracking data are available via contacting the corresponding author (longyang@princeton.edu).

References

Berne, A., G. Delrieu, J.-D. Creutin, and C. Obled (2004), Temporal and spatial resolution of rainfall measurements required for urban hydrology, *J. Hydrol.*, *299*, 166–179.

Chappell, C. F. (1986), Quasi-stationary convective events, in *Mesoscale Meteorology and Forecasting*, edited by P. F. Ray, Am. Meteorol. Soc., Washington, D. C.

Corfidi, S. F. (2003), Cold pools and MCS propagation: Forecasting the motion of downwind-developing MCSs, *Weather Forecasting*, *18*, 997–1017.

Cotton, W. R., and R. A. Anthes (1989), *Storm and Cloud Dynamics*, *Intl. Geophys. Ser.*, vol. 44, Academic Press, New York.

Davis, R. S. (2001), Flash flood forecast and detection methods, *Meteorol. Monogr.*, *28*(50), 481–526.

Dixon, M., and G. Wiener (1993), TITAN: Thunderstorm Identification, Tracking, Analysis, and Nowcasting—A radar-based methodology, *J. Atmos. Oceanic Technol.*, *10*(6), 785–797.

Doswell, C. A., H. E. Brooks, and R. A. Maddox (1996), Flash flood forecasting: An ingredients-based methodology, *Weather Forecasting*, *11*(4), 560–581.

Engelbrecht, H. H., and G. N. Brancato (1959), World record one-minute rainfall at Unionville, Maryland, *Mon. Weather Rev.*, *87*(8), 303–306.
Gallus, W. A., N. A. Snook, and E. V. Johnson (2008), Spring and summer severe weather reports over the midwest as a function of convective mode: A preliminary study, *Weather Forecasting*, *23*(1), 101–113.
Goodman, S. J., D. E. Buechler, P. D. Wright, and W. David (1988), Lightning and precipitation history of a microburst-producing storm, *Geophys. Res. Lett.*, *15*(11), 1185–1188, doi:10.1029/GL015i011p01185.
Hamada, A., Y. N. Takayabu, C. Liu, and E. J. Zipser (2015), Weak linkage between the heaviest rainfall and tallest storms, *Nat. Commun.*, *6*, 6213, doi:10.1038/ncomms7213.
Holle, R. L., and S. P. Bennett (1997), Lightning ground flashes associated with summer 1990 flash floods and stream flow in Tucson, Arizona: An exploratory study, *Mon. Weather Rev.*, *125*, 1526–1536.
Houze, R. A., K. L. Rasmussen, S. Medina, S. R. Brodzik, and U. Romatschke (2011), Anomalous atmospheric events leading to the summer 2010 floods in Pakistan, *Bull. Am. Meteorol. Soc.*, *92*(3), 291–298.
Intergovernmental Panel on Climate Change (2007), *Climate Change 2007: The Physical Science Basis. Contribution of Working Group I to the Fourth Assessment Report of the Intergovernmental Panel on Climate Change*, Cambridge Univ. Press, Cambridge, U. K., and New York.
Javier, J. R. N., J. A. Smith, J. England, M. L. Baeck, M. Steiner, and A. A. Ntelekos (2007), Climatology of extreme rainfall and flooding from orographic thunderstorm systems in the upper Arkansas River basin, *Water Resour. Res.*, *43*, W10410, doi:10.1029/2006WR005093.
Krehbiel, P. R. (1986), *The Electric Structure of Thunderstorms*, The National Academies Press, Washington, D. C.
Lin, Y., and K. E. Mitchell (2005), The NCEP stage II/IV hourly precipitation analyses: Development and applications. Preprints, in *19th Conference on Hydrology*, Am. Meteorol. Soc., San Diego, Calif.
Maddox, R. A., C. F. Chappell, and L. R. Hoxit (1979), Synoptic and meso-α scale aspects of flash flood events, *Bull. Am. Meteorol. Soc.*, *60*(2), 115–123.
Mesinger, F., G. DiMego, E. Kalnay, K. Mitchell, P. C. Shafran, W. Ebisuzaki, D. Jovic, J. Woollen, E. Rogers, and E. H. Berbery (2006), North American regional reanalysis, *Bull. Am. Meteorol. Soc.*, *87*(3), 343–360.
Morin, E., D. C. Goodrich, R. A. Maddox, X. Gao, H. V. Gupta, and S. Sorooshian (2006), Spatial patterns in thunderstorm rainfall events and their coupling with watershed hydrological response, *Adv. Water Resour.*, *29*, 843–860.
National Research Council (2012), *Urban Meteorology: Forecasting, Monitoring, and Meeting Users' Needs*, National Academies Press, Washington, D. C.
Ntelekos, A. A., K. P. Georgakakos, and W. F. Krajewski (2006), On the uncertainties of flash flood guidance: Toward probabilistic forecasting of flash floods, *J. Hydrometeorol.*, *7*, 896–915.
Ntelekos, A. A., J. A. Smith, and W. F. Krajewski (2007), Climatological analyses of thunderstorms and flash floods in the Baltimore metropolitan region, *J. Hydrometeorol.*, *8*(1), 88–101.
Ntelekos, A. A., J. A. Smith, M. L. Baeck, W. F. Krajewski, A. J. Miller, and R. Goska (2008), Extreme hydrometeorological events and the urban environment: Dissecting the 7 July 2004 thunderstorm over the Baltimore MD metropolitan region, *Water Resour. Res.*, *44*, W08446, doi:10.1029/2007WR006346.
Ogden, F. L., N. R. Pradhan, C. W. Downer, and J. A. Zahner (2011), Relative importance of impervious area, drainage density, width function, and subsurface storm drainage on flood runoff from an urbanized catchment, *Water Resour. Res.*, *47*, W12503, doi:10.1029/2011WR010550.
Orville, R. E., and G. R. Huffines (2001), Cloud-to-ground lightning in the United States: NLDN results in the first decade, 1989–98, *Mon. Weather Rev.*, *129*(5), 1179–1193.
Peleg, N., and E. Morin (2012), Convective rain cells: Radar-derived spatio-temporal characteristics and synoptic patterns over the Eastern Mediterranean, *J. Geophys. Res.*, *117*, D15116, doi:10.1029/2011JD017353.
Peters, J. M., and R. S. Schumacher (2014), Mechanisms for organization and echo training in a flash-flood-producing mesoscale convective system, *Mon. Weather Rev.*, *143*, 1058–1085.
Petersen, W. A., and S. A. Rutledge (1998), On the relationship between cloud-to-ground lightning and convective rainfall, *J. Geophys. Res.*, *103*(D12), 14,025–14,040, doi:10.1029/97JD02064.
Petersen, W. A., L. D. Carey, S. A. Rutledge, J. C. Knievel, N. J. Doesken, R. H. Johnson, T. B. McKee, T. V. Haar, and J. F. Weaver (1999), Mesoscale and radar observations of the Fort Collins flash flood of 28 July 1997, *Bull. Am. Meteorol. Soc.*, *80*(2), 191–216.
Rasmussen, B. K. L., A. J. Hill, V. E. Toma, M. D. Zuluaga, and P. J. Webster (2014), Multiscale analysis of three consecutive years of anomalous flooding in Pakistan, *Q. J. R. Meteorol. Soc.*, *141*(689), 1259–1276.
Schumacher, R. S., and R. H. Johnson (2004), Organization and environmental properties of extreme-rain-producing mesoscale, *Mon. Weather Rev.*, *133*, 961–976.
Smith, B. K., and J. A. Smith (2015), The flashiest watersheds in the contiguous United States, *J. Hydrometeorol.*, 150904104740009, doi:10.1175/JHM-D-14-0217.1.
Smith, J. A., M. L. Baeck, Y. Zhang, and C. A. Doswell (2001), Extreme rainfall and flooding from supercell thunderstorms, *J. Hydrometeorol.*, *2*(5), 469–489.
Smith, J. A., A. J. Miller, M. L. Baeck, P. A. Nelson, G. T. Fisher, and K. L. Meierdiercks (2005), Extraordinary flood response of a small urban watershed to short-duration convective rainfall, *J. Hydrometeorol.*, *6*(5), 599–617.
Smith, J. A., E. Hui, M. Steiner, M. L. Baeck, W. F. Krajewski, and A. A. Ntelekos (2009), Variability of rainfall rate and raindrop size distributions in heavy rain, *Water Resour. Res.*, *45*, W04430, doi:10.1029/2008WR006840.
Smith, J. A., M. L. Baeck, G. Villarini, and W. F. Krajewski (2010), The hydrology and hydrometeorology of flooding in the Delaware river basin, *J. Hydrometeorol.*, *11*(4), 841–859.
Smith, J. A., G. Villarini, and M. L. Baeck (2011), Mixture distributions and the hydroclimatology of extreme rainfall and flooding in the eastern United States, *J. Hydrometeorol.*, *12*(2), 294–309.
Smith, J. A., M. L. Baeck, G. Villarini, C. Welty, A. J. Miller, and W. F. Krajewski (2012), Analyses of a long-term, high-resolution radar rainfall data set for the Baltimore metropolitan region, *Water Resour. Res.*, *48*, W04504, doi:10.1029/2011WR010641.
Steiner, M., R. A. Houze, and S. E. Yuter (1995), Climatological characterization of three-dimensional storm structure from operational radar and rain gauge data, *J. Appl. Meteorol.*, *34*(9), 1978–2007.
Syed, K. H., D. C. Goodrich, D. E. Myers, and S. Sorooshian (2003), Spatial characteristics of thunderstorm rainfall fields and their relation to runoff, *J. Hydrol.*, *271*, 1–21.
Tapia, A., J. A. Smith, and M. Dixon (1998), Estimation of convective rainfall from lightning observations, *J. Appl. Meteorol.*, *37*(11), 1497–1509.
Tattelman, P., and P. T. Willis (1985), Model vertical profiles of extreme rainfall rate, liquid water content and drop-size distribution, Air Force Geophys. Lab., Tech. Rep. 85-0200, Hanscomb Air Force Base, MA, 34 pp.
Villarini, G., J. A. Smith, F. Serinaldi, J. Bales, P. D. Bates, and W. F. Krajewski (2009), Flood frequency analysis for nonstationary annual peak records in an urban drainage basin, *Adv. Water Resour.*, *32*(8), 1255–1266.

Willis, P. T., and P. Tattelman (1989), Drop-size distributions associated with intense rainfall, *J. Appl. Meteorol.*, *28*, 3–15.
Wright, D. B., J. A. Smith, G. Villarini, and M. L. Baeck (2012), Hydroclimatology of flash flooding in Atlanta, *Water Resour. Res.*, *48*, W04524, doi:10.1029/2011WR011371.
Yang, G., L. C. Bowling, K. A. Cherkauer, and B. C. Pijanowski (2011), The impact of urban development on hydrologic regime from catchment to basin scales, *Landscape Urban Plann.*, *103*(2), 237–247.
Yang, L., J. A. Smith, D. B. Wright, M. L. Baeck, G. Villarini, F. Tian, and H. Hu (2013a), Urbanization and climate change: An examination of nonstationarities in urban flooding, *J. Hydrometeorol.*, *14*(6), 1791–1809.
Yang, L., J. A. Smith, M. L. Baeck, E. Bou-Zeid, S. M. Jessup, F. Tian, and H. Hu (2013b), Impact of urbanization on heavy convective precipitation under strong large-scale forcing: A case study over the Milwaukee–Lake Michigan region, *J. Hydrometeorol.*, *15*(1), 261–278.
Yang, L., F. Tian, and D. Niyogi (2015), A need to revisit hydrologic responses to urbanization by incorporating the feedback on spatial rainfall patterns, *Urban Clim.*, *12*, 128–140.
Yeung, J., J. A. Smith, G. Villarini, A. A. Ntelekos, M. L. Baeck, and W. F. Krajewski (2011), Regional precipitation climatology of the NewYork—New Jersey Metropolitan Region, *Adv. Water Resour.*, *34*(2), 21.
Yeung, J. K., J. A. Smith, M. L. Baeck, and G. Villarini (2015), Lagrangian analyses of rainfall structure and evolution for organized thunderstorm systems in the urban corridor of the Northeastern US, *J. Hydrometeorol.*, *16*(4), 1575–1595.
Zhang, Y., J. A. Smith, A. A. Ntelekos, M. L. Baeck, W. F. Krajewski, and F. Moshary (2009), Structure and evolution of precipitation along a cold front in the Northeastern United States, *J. Hydrometeorol.*, *10*(5), 1243–1256.
Zipser, E. J., and K. R. Lutz (1994), The vertical profile of radar reflectivity of convective cells: A strong indicator of storm intensity and lightning probability?, *Mon. Weather Rev.*, *122*, 1751–1759.
Zipser, E. J., D. J. Cecil, C. Liu, S. W. Nesbitt, and D. P. Yorty (2006), Where are the most intense thunderstorms on Earth?, *Bull. Am. Meteorol. Soc.*, *87*(8), 1057–1071.